

First local helioseismic experiments with CO⁵BOLD

O. Steiner^{1,*}, G. Vigeesh², L. Krieger^{1,2}, S. Wedemeyer-Böhm³, W. Schaffenberger¹, and B. Freytag⁴

¹ Kiepenheuer-Institut für Sonnenphysik, Schöneckstrasse 6, D-79104 Freiburg, Germany

² Indian Institute of Astrophysics, Koramangala, Bangalore 560034, India

³ Institute of Theoretical Astrophysics, University of Oslo, P.O. Box 1029 Blindern, N-0315 Oslo, Norway

⁴ Centre de Recherche Astronomique de Lyon - Ecole Normale Supérieure, 46, Allée d'Italie, F-69364 Lyon Cedex 07, France

Received 2006 Dec 30, accepted 2007 Jan 2

Published online 2007 Feb 28

Key words Sun: helioseismology – Sun: magnetic fields – Sun: chromosphere

With numerical experiments we explore the feasibility of using high frequency waves for probing the magnetic fields in the photosphere and the chromosphere of the Sun. We track a plane-parallel, monochromatic wave that propagates through a non-stationary, realistic atmosphere, from the convection-zone through the photosphere into the magnetically dominated chromosphere, where it gets refracted and reflected. We compare the wave travel time between two fixed geometrical height levels in the atmosphere (representing the formation height of two spectral lines) with the topography of the surface of equal magnetic and thermal energy density (the magnetic canopy or $\beta = 1$ contour) and find good correspondence between the two. We conclude that high frequency waves indeed bear information on the topography of the ‘magnetic canopy’.

© 2007 WILEY-VCH Verlag GmbH & Co. KGaA, Weinheim

1 What is CO⁵BOLD?

CO⁵BOLD is a computer code designed for simulating hydrodynamic processes including radiative transfer in the outer and inner layers of stars. Additionally, it can treat the interaction of magnetic fields with a plasma in the magnetohydrodynamic (MHD) approximation, non-equilibrium chemical reaction networks, dynamic hydrogen ionization, and dust formation in stellar atmospheres. CO⁵BOLD stands for COnservative COde for the COmputation of COmpressible COnvection in a BOx of L Dimensions with $L = 2, 3$.

In the past few years, CO⁵BOLD has been extensively used for ‘box in a star’ computations (for a review see Steffen 2007), where a small piece of a star’s interior and/or atmosphere is simulated. A typical result of these kinds of computations is the emergent intensity from the stellar surface. In this way, the surface granulation pattern of the Sun and other stars, e.g., A stars (Kochukhov et al. 2006) or red giants have been simulated. In the case of the Sun, a detailed comparison between high resolution observation and simulation is possible and allows for a validation of the latter (Steffen, Ludwig & Freytag 2002). On the other hand, CO⁵BOLD is also used for ‘star in a box’ computations in which the computational box contains an entire star, e.g., the red supergiant Betelgeuse (Freytag, Steffen & Dorch 2002; Chiavassa et al. 2006).

Recent applications of CO⁵BOLD focus on the dynamical evolution of carbon monoxide in the solar photosphere

(Wedemeyer-Böhm et al. 2005; Wedemeyer-Böhm & Steffen 2007) and on the dynamical hydrogen ionization (Leenaarts & Wedemeyer-Böhm 2006), where deviations from statistical ionization equilibrium occur. These works have been carried out in connection with efforts for a simulation including the layers from the convection zone to the chromosphere of the Sun (Wedemeyer et al. 2004), which now have been expanded in order to include the effects of magnetic fields (Schaffenberger et al. 2005, 2006). Details of these MHD-simulations are given in the next section.

CO⁵BOLD works with Cartesian, non-equidistant but static grids, realistic equations of state, multidimensional radiation transfer, realistic opacities, and it features various boundary conditions. As a simplest option the radiative transfer can be treated frequency-independently (‘grey’). Alternatively, the frequency-dependence can be taken into account by using a multi-group scheme that solves the radiative transfer problem for different opacity groups, which takes effects of line blanketing into account.

The multidimensional problem is reduced to 1-D problems by dimensional splitting. Each of these 1-D problems is solved with a Godunov-type finite-volume scheme using an approximate Riemann solver modified for a general equation of state and gravity. A Roe-type approximate Riemann solver is used for integration of the hydrodynamic equations, whereas in the case of the MHD-equations we use a HLL-solver of second order accuracy, instead. More details on the MHD-solver can be found in Schaffenberger et al. (2005). A good introduction to the above mentioned numerical techniques can be found in Laney (1998),

* Corresponding author: steiner@kis.uni-freiburg.de

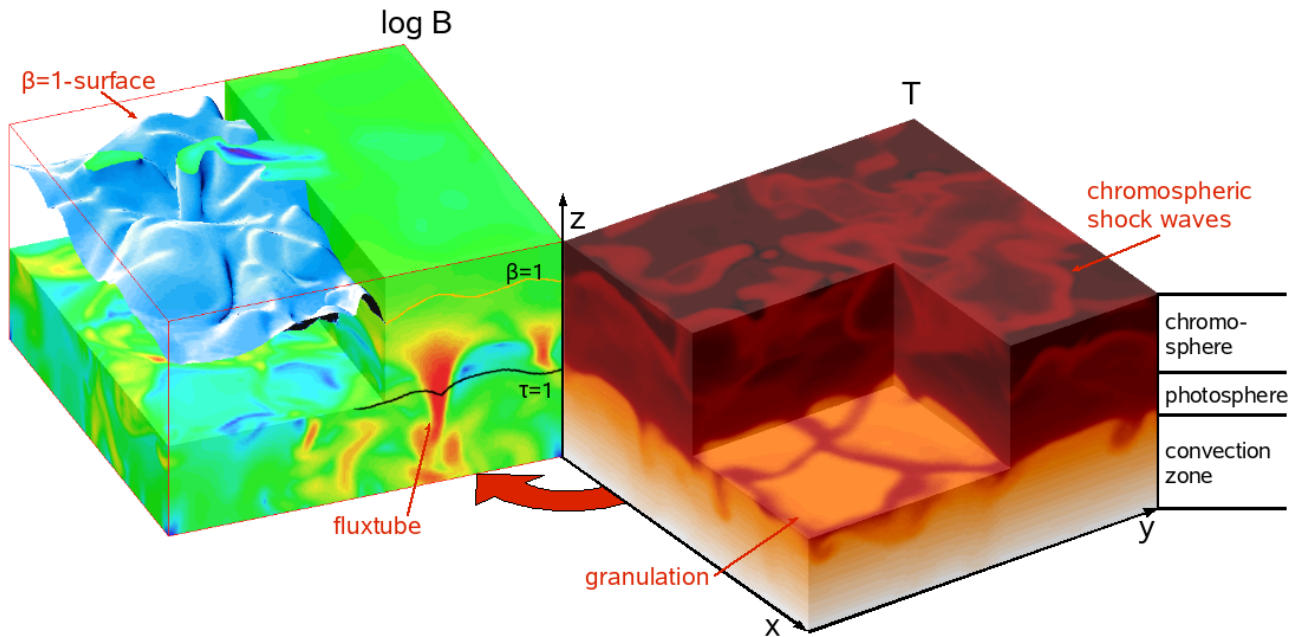


Fig. 1 *Left:* Magnetic flux density on a color scale, where red signifies strong (greater or approximately 0.1 T) and blue weak fields. The surface of equipartition between magnetic and thermal energy density ($\beta = 1$) is indicated as blue surface (on the lateral boundaries by a yellow curve). The black curve indicates optical depth unity. *Right:* The temperature in colors shows granules and cool intergranular downflows at a height that corresponds to the mean optical depth unity. Note the mesh-work like pattern of hot shock waves in the chromospheric layers. From Wedemeyer-Böhm (2007).

LeVeque (2002), LeVeque et al. (1998), or Toro (1999). CO⁵BOLD is programmed in FORTRAN 90 with OpenMP directives. The manual for CO⁵BOLD can be found under www.astro.uu.se/~bf/co5bold_main.html while talks delivered at the first CO⁵BOLD workshop are at http://folk.uio.no/svenwe/cws2006/cws_cont.html. For the analysis and visualization a CO⁵BOLD analysis tool (CAT, <http://folk.uio.no/svenwe/co5bold/cat.html>) exists.

2 MHD-simulation from the convection zone to the chromosphere

A three-dimensional magnetohydrodynamic simulation of the integral layers from the upper convection zone to the middle chromosphere was carried out by Schaffenberger et al. (2005, 2006). The computational domain in this simulation extends over a height range of 2800 km, of which 1400 km reach below the mean surface of optical depth unity and 1400 km above it. The horizontal dimensions are 4800 km \times 4800 km. With 120^3 grid cells, the spatial resolution in the horizontal direction is 40 km, while in the vertical direction it is 50 km through the convection-zone layer and 20 km throughout the photosphere and chromosphere. The lateral boundary conditions are periodic in all variables, whereas the lower boundary is ‘open’ in the sense that the fluid can freely flow in and out of the computational domain under the condition of vanishing total mass flux. The specific entropy of the inflowing mass is fixed to a value previously determined so as to yield solar radiative flux at the

upper boundary. The upper boundary can be chosen to be transmitting so that acoustic waves can leave the computational domain with no significant reflection at the boundary. Stress-free conditions are in effect for the horizontal velocities, viz., $dv_{x,y}/dz = 0$.

The MHD simulation starts with a homogeneous, vertical, unipolar magnetic field of a flux density of 0.001 T (10 G) superposed on a previously computed, relaxed model of thermal convection. This flux density is thought to mimic magnetoconvection in a very quiet network-cell interior. The magnetic field is constrained to have vanishing horizontal components at the top and bottom boundary but lines of force can freely move in the horizontal direction, allowing for flux concentrations to extend right to the boundaries. Although this condition is quite stringent, especially at the top boundary, it still allows the magnetic field to freely expand with height through the photospheric layers into the more or less homogeneous chromospheric field, different from conventional simulations that extend to a height of typically 600 km, only.

Subsequent to superposition of the magnetic field, flux expulsion from the granule centers takes place and within less than 5 minutes, the magnetic field concentrates in narrow sheets and small knots near the surface of optical depth unity with field strengths up to approximately 1 kG. Occasionally, these magnetic flux concentrations extend down to the bottom boundary at a depth of 1400 km but more often, they disperse again at a depth of less than 1000 km leaving

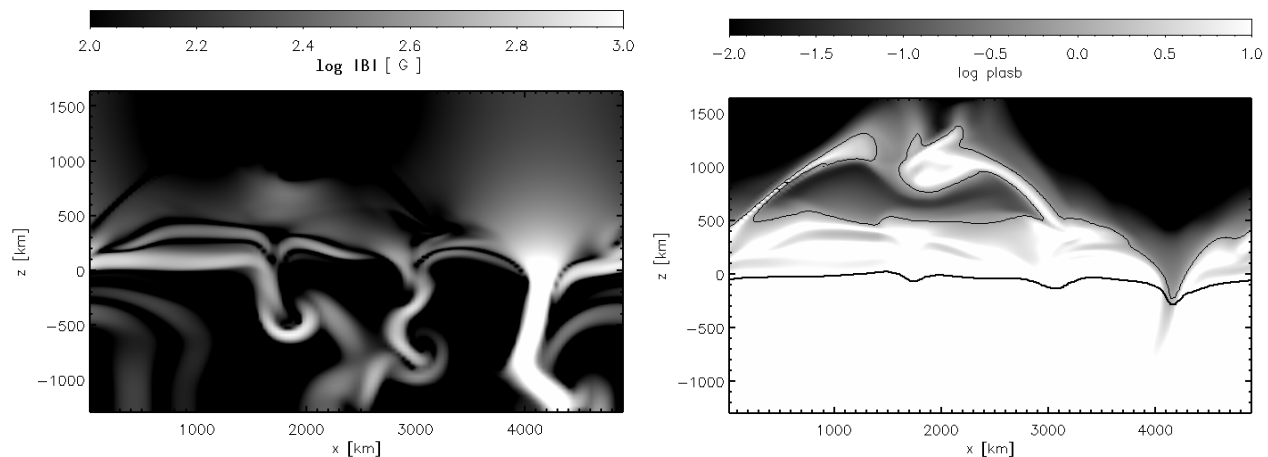


Fig. 2 Still images from a time series for the instant $t = 1368$ s after starting with an initial homogeneous vertical field of 100 G. *Left:* Logarithmic magnetic flux density. *Right:* Logarithm of the ratio of thermal to magnetic energy density (plasma- β). Also shown are the contour of $\beta = 1$ (thin curve) and the surface of optical depth unity, $\tau_{500\text{ nm}} = 1$. A strong magnetic flux sheet has formed near $x = 4000$ km that causes the funnel of low β visible in the right hand panel.

flux concentrations of a strength of a few hundred Gauss only.

Figure 1 gives a synoptic summary of phenomena that occur in this simulation. The box on the left hand side renders the logarithm of the magnetic flux density on a color scale, where red signifies strong (greater or approximately 0.1 T) and blue weak fields. The surface of equipartition between magnetic and thermal energy density ($\beta = 1$) is indicated as blue surface and on the front side by a yellow curve. It is corrugated and continuously changes shape on a time-scale of a few minutes. The black curve indicates optical depth unity. One can see that close to the front side boundary, a magnetic flux concentration has formed. It leads to a small dip in the surface of optical depth unity due to the reduced density within the flux concentration compared to the density in the environment at the same geometrical height. The box on the right hand side shows the temperature in colors. We see granules (yellow to light red) near the height that corresponds to optical depth unity and a network of cool (dark red) intergranular downflows. In the chromosphere exists a dynamic, mesh-work like pattern of hot shock waves with cool post-shock regions in between.

3 Local helioseismic experiments with high frequency waves

Classical helioseismic tools usually rely on the analysis of waves with frequencies below the acoustic cutoff that are essentially trapped in the internal acoustic cavity of the Sun. These waves are largely evanescent in the outer atmosphere and carry little information on this region. The situation changes for waves with frequencies above the acoustic cutoff frequency that can freely propagate in the atmosphere. When they encounter a change in the dispersive character-

istics of the medium, they are refracted and reflected (Finsterle et al. 2004).

This effect has been employed by Finsterle et al. (2004) in order to obtain the three-dimensional topography of the ‘magnetic canopy’ in and around active regions by determining the propagation behavior of high-frequency acoustic waves in the solar chromosphere. Their method bears considerable potential for the exploration of the magnetic field in the solar atmosphere by helioseismological means.

In order to test the reliability and to further explore and assess this method we have carried out a first series of two-dimensional MHD-simulations of the propagation of high frequency waves through a magnetically structured, realistic atmosphere. We start with a simulation very similar to that described in the previous section, but carried out in a two-dimensional computational domain of 4900 km width and spanning a height range of 2900 km, of which 1300 km reach into the convection zone and 1600 km above the average level of optical depth unity.

Since we start with a mean magnetic flux density of 10 G and 100 G, the magnetic structures that form in the course of time represent magnetic fields in a very quiet network cell interior and in the magnetic network, respectively, rather than the active region fields observed by Finsterle et al. (2004). Also, different from active region fields, this field evolves on the much shorter time scale of granular evolution. Therefore, and for reasons of computational costs, we do not analyze a long duration time series as is normally necessary in local helioseismology. Instead, we introduce a velocity perturbation of given frequency and amplitude at the bottom of the computational domain with which we generate a monochromatic, plane parallel wave that propagates within a time span of about 200 s across the height range of the computational domain. Experiments with various amplitudes and frequencies have been carried out. In the follow-

ing, however, we only use the values stated in connection with Eq. (1).

We then determine the arrival time of the wave front at three different heights in the atmosphere that should roughly represent the heights of maximal Doppler response of the spectral lines Ni I 676.8 nm at 200 km, K I 769.9 nm at 420 km, and Na I 589.0 nm at 800 km (Finsterle et al. 2004). Subsequently, we compute the travel times between these heights. They are thought to become modified through the presence of a strong magnetic field in the sense that a strong magnetic field reduces the travel time. At this stage we do not carry out radiation transfer for computing the response of spectral lines to the perturbation but simply determine the velocity at the corresponding (fixed) line-formation heights in the computational box for determining the arrival time of the wave front. The wave front is detected when the velocity perturbation surpasses a height dependent velocity threshold of less than 100 m/s.

In the following we consider the time span from $t = 1200$ s to $t = 1400$ s of a simulation that started with a homogeneous vertical field of 100 G at $t = 0$ s. Figure 2 shows a snapshot of the instant $t = 1368$ s. The panel on the left hand side shows the logarithmic magnetic flux density, where the values in Gauss are indicated in the grey-scale bar in the top margin of the figure. A strong magnetic flux sheet has formed near $x = 4000$ km. It leads to a dip in the surface of optical depth unity, visible in the panel on the right hand side. There, also the contour of $\beta = 1$, where $\beta = p_{\text{gas}}/(B^2/8\pi)$, i.e., the contour of equipartition of thermal and magnetic energy density, is indicated. The magnetic flux concentration causes a funnel of low β .

The $\beta = 1$ contour delimits the transition from the weak to the strong field regime. In the latter regime the magnetic field dominates over thermal pressure. The gas pressure exponentially decreases with height in a gravitationally stratified atmosphere but the magnetic pressure can only decrease to a lower limit set by the initial average flux density. Once the magnetic field, which may be concentrated in small tubes and sheets in the deep photosphere, has expanded to completely fill the available space, it cannot further expand and its strength remains essentially constant with height. Therefore, β unabatedly decreases with height so that with increasing height the atmosphere becomes sooner or later magnetically dominated. Correspondingly, the $\beta = 1$ contour in Fig. 2 (right) extends in a more or less horizontal direction at a height of 500 km with the exceptions of the location of the strong flux sheet, where it dips even below $z = 0$, and two islands higher up in the atmosphere, caused by chromospheric shock waves.

The $\beta = 1$ contour also marks the region of wave transmission and conversion (Rosenthal et al. 2002; Bogdan et al. 2003; Cally 2007). For example an incident acoustic plane wave converts to a fast magnetic wave and gets reflected back into the atmosphere. This effect is visible in Fig. 3, which shows, from bottom to top, a time sequence of a plane wave traveling through the magnetically structured

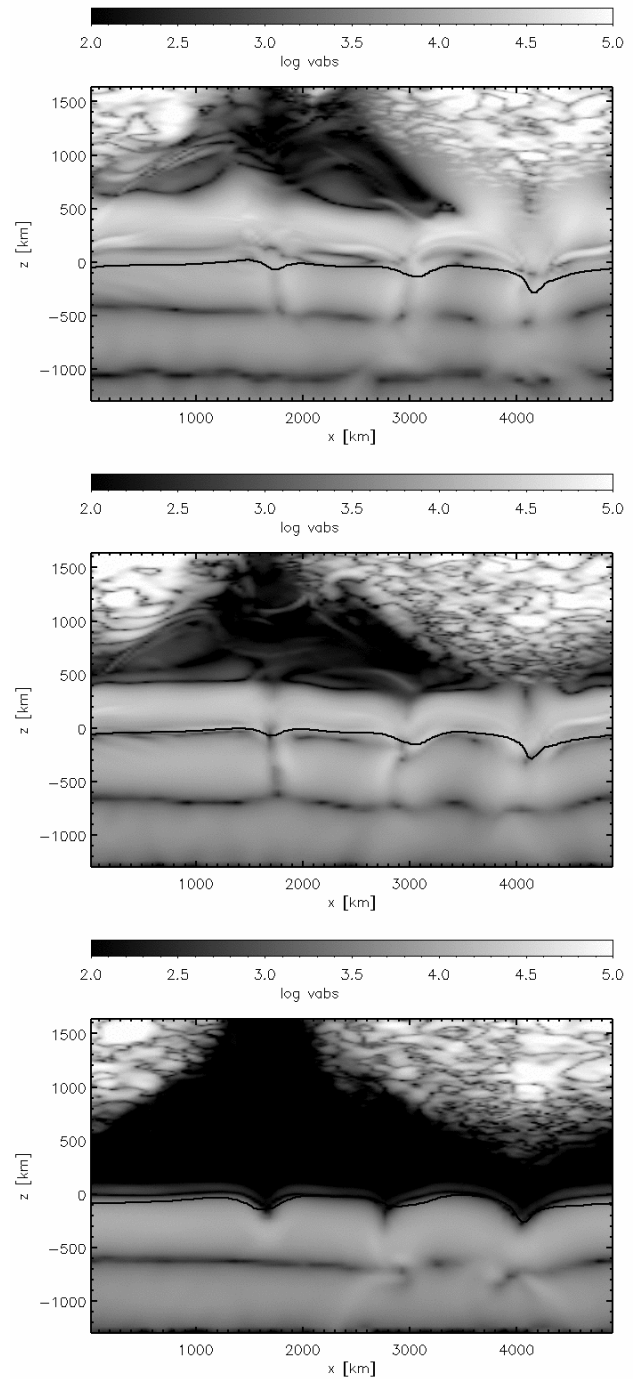


Fig. 3 A plane parallel wave with frequency 20 mHz travels through convecting plasma into the magnetically structured photosphere and further into the low β (magnetically dominated) chromosphere. The three panels show the difference in absolute velocity between the perturbed and the unperturbed solution 100 s, 148 s, and 168 s (from bottom to top) after the start of the perturbation (Eq. 1). Magnetic field and plasma β corresponding to the instant of the top panel are given in Fig. 2. A spurious velocity signal that is believed to have numerical origin dominates the very low β region in the upper right and upper left corners. The horizontally running black curve near $z = 0$ indicates optical depth $\tau_{500 \text{ nm}} = 1$. The velocity scaling is logarithmic with dimension cm/s.

and simultaneously evolving atmosphere of Fig. 2. In order to visualize the wave we have run the simulation twice from $t = 1200$ s to $t = 1400$ s, once without perturbation and once with a velocity perturbation at the bottom of the computational domain of the form

$$v_z(t) = v_0 \sin(2\pi(t - t_0)\nu), \quad (1)$$

where v_0 was chosen to be 0.05 km/s and $\nu = 20$ mHz. The two runs were carried out with identical time stepping. Following that, the two velocity fields are subtracted, which then reveals the wave perturbation that travels on top of the non-stationary evolving convective motion.

Due to a numerical problem of unknown origin, considerable spurious velocities occur in the region of very low plasma- β in the chromospheric layers of the magnetic flux concentration. This problem will be addressed in a next stage of the present project. Nevertheless, we can clearly observe the following phenomena. Initially the wave front is retarded at the location of the flux concentration (at $x \approx 4000$ km) because of the lower temperature of the plasma within the flux concentration, hence the lower sound speed (bottom panel, 100 s after start of the perturbation). It undergoes acceleration when entering the funnel of $\beta < 1$ so that the wave within the funnel is now leading 148 s after start of the perturbation (middle panel). At the same time the wave becomes fast magnetic in character and starts to refract. Thus, the wave front becomes inclined until aligned with the vertical direction and it further turns until traveling into the downward direction. In the top panel, only 20 s later, the wave front in the low- β funnel (extending from $(x, z) = (2400, 1500)$ to $(3400, 500)$) has already completely turned around and travels back *into* the atmosphere. Therefore, we can speak of a reflection of the magnetic wave in the low- β region. A similar fanning out of the wave front occurs around $x = 1400$ km when it reaches the ‘canopy’-height where $\beta = 1$ at about 500 km.

Clearly, the travel time for the wave in the low- β region is much smaller than elsewhere. Figure 4 shows the travel time between the line formation heights of Ni I 676.8 nm at 200 km and K I 769.9 nm at 420 km (thick solid curve) as a function of horizontal distance, x . The time axis is given on the left hand side. Superposed on this plot is the contour of $\beta = 1$ (dash-dotted curve), where the height in the atmosphere is given by the z -axis on the right hand side. Clearly, the travel-time curve follows the dip of the β -contour at the location of the flux concentration, which demonstrates that a mapping of the $\beta = 1$ surface by helioseismic methods is in principle possible.

Because of the spurious velocity noise in the region of very low β , we were unable to reliably determine the wave-front arrival at the line-formation height of Na I D2 589.0 nm at 800 km. But we expect for the travel time difference between 800 and 420 km an even more pronounced dip at the location of the magnetic flux concentration than for the difference between 200 and 420 km.

We have also carried out a similar simulation with an initial vertical field of 10 G flux density. Because of the

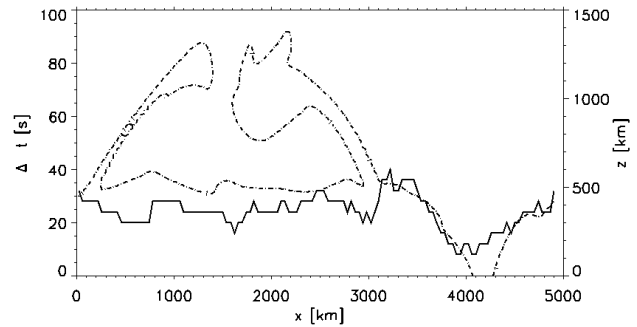


Fig. 4 Wave travel time across the layer from $z = 200$ km to $z = 420$ km as a function of horizontal distance (thick solid curve). Superposed is the contour of $\beta = 1$ (magnetic and thermal equipartition), for which the height is indicated in the right hand side ordinate (dash-dotted curve). Note that the travel time markedly decreases where the low β region intrudes this layer.

lower field strength the average height where $\beta = 1$ (canopy height) is in this case at approximately 1000 km compared to 500 km in the case of 100 G. We could think of the two simulations with 10 G and 100 G initial field strength representing very quiet network interior and network regions, respectively. Examination of the travel times for 20 mHz waves reveals no major difference in the layer from 200 km to 420 km. In the 100 G case the mean travel time is 23.9 s and 25.7 s when excluding the strong flux concentration that has formed at $x \approx 4000$ km. The corresponding time in the 10 G case is 28.0 s. Since this layer is *below* the canopy in both cases, there is only a small difference in wave travel-time. However, for the layer from 420 km to 800 km we obtain in the 100 G case a travel time of 25.1 s (when excluding the strong flux concentration, where reliable values are unavailable). The corresponding travel time in the 10 G case is 39.2 s, much longer because in this case this layer is still below the low- β regime while it is entirely inside it in the 100 G case. Again this demonstrates that measurements of the wave travel-time can differentiate between network and internetwork regions.

4 Conclusions

We have carried out local helioseismic experiments using the magnetohydrodynamic code CO⁵BOLD. A plane-parallel monochromatic wave perturbation that is generated at the bottom of the computational domain within the convection zone propagates into a non-stationary, realistic atmosphere that extends up into the middle chromosphere. There, it enters a regime in which the magnetic energy density surpasses the thermal energy density and converts from acoustic to magnetic in nature. It is experimentally demonstrated how a magnetic flux concentration leads to refraction and reflection of the wave.

The experiments also reveal a numerical problem of unknown origin. Two runs that are identical with the exception of the wave perturbation at the bottom of the computational

domain show considerable differences in the velocity field in regions of $\beta \ll 10^{-2}$ from the very beginning. In these tenuous regions, smallest pressure imbalances that may occur because of the thermal energy density being only a small fraction of the total energy density there, must lead to large accelerations.

We show that the wave travel-time between two fixed levels in the atmosphere bears information on the nature of the wave and consequently on the magnetic field. The travel time is reduced in regions of low β (strong magnetic field). For a monochromatic wave of frequency 20 mHz we demonstrate with Fig. 4 that the travel time between the heights of 200 and 420 km in seconds times 15 matches approximately the height of the $\beta = 1$ surface in km. In particular, the travel-time curve delineates a funnel of low β that is caused by a local magnetic flux concentration.

The region and magnetic structure considered in the present simulation is much smaller than the active region observed by Finsterle et al. (2004) and we use 20 mHz waves, instead of the 7 mHz employed by Finsterle et al. (2004). Also, by using plane parallel waves we assume the wave coherence to be always larger than the magnetic structure under investigation. Subject to these reservations, the numerical experiments carried out in this paper support the conclusions of Finsterle et al. (2004) and their proposition using high frequency waves for mapping the magnetic topography in the chromosphere.

Acknowledgements. The authors are very grateful to M. Haberreiter and R. Hammer for detailed comments on a draft of this paper. This work was supported by the Deutsche Forschungsgemeinschaft (DFG), grant Ste 615/5, the German Academic Exchange Service (DAAD), grant D/05/57687, and the Indian Department of Science & Technology (DST), grant DST/INT/DAAD/P146/2006. Participation of O. S. at the HELAS workshop in Nice was supported by the European Helio- and Asteroseismology Network (HELAS), which is funded by the European Union's Sixth Framework Programme.

References

- Bogdan, T.J., Carlsson, M., Hansteen, V.H., et al.: 2003, ApJ 599, 626
- Cally, P.S.: 2007, AN, this volume
- Chiavassa, A., Plez, B., Josselin, E., Freytag, B.: 2006, EAS Publ. Series 18, p. 177
- Finsterle, W., Jefferies, S.M., Cacciani, A., Rapex, P., McIntosh, S.W.: 2004, ApJ 613, L185
- Freytag, B., Steffen, M., Dorch, B.: 2002, AN 323, 213
- Kochukhov, O., Freytag, B., Piskunov, N., Steffen, M.: 2006, in: F. Kupka, I.A. Roxburgh, K.L. Chan (eds.), *Convection in Astrophysics*, IAU Symp. 239, p. 41
- Laney, C.B.: 1998, *Computational Gasdynamics*, Cambridge University Press, Cambridge
- Leenaarts, J., Wedemeyer-Böhm, S.: 2006, A&A 460, 301
- LeVeque, R.J.: 2002, *Finite Volume Methods for Hyperbolic Problems*, Cambridge University Press, Cambridge
- LeVeque, R.J., Mihalas, D., Dorfi, E.A., Müller, E.: 1998, *Computational Methods for Astrophysical Fluid Flows*, Springer, Berlin
- Rosenthal, C.S., Bogdan, T.J., Carlsson, M., et al.: 2002, ApJ 564, 508
- Schaffnerberger, W., Wedemeyer-Böhm, S., Steiner, O., Freytag, B.: 2005, in: D.E. Innes, A. Lagg, S.K. Solanki (eds.), *Chromospheric and Coronal Magnetic Fields*, ESA SP-596, p. 65.1
- Schaffnerberger, W., Wedemeyer-Böhm, S., Steiner, O., Freytag, B.: 2006, in: H. Uitenbroek, J. Leibacher, R.F. Stein (eds.), *Solar MHD Theory and Observation: A High Spatial Resolution Perspective*, ASP Conf. Ser. 354, p. 351
- Steffen, M.: 2007, in: F. Kupka, I.A. Roxburgh, K.L. Chan (eds.), *Convection in Astrophysics*, IAU Symp. 239, in press
- Steffen, M., Ludwig, H.-H., Freytag, B.: 2002, AN Suppl. 324, 174
- Toro, E.F.: 1999, *Riemann Solvers and Numerical Methods for Fluid Dynamics*, Springer, Berlin
- Wedemeyer-Böhm, S.: 2007, in: F. Kupka, I.A. Roxburgh, K.L. Chan (eds.), *Convection in Astrophysics*, IAU Symp. 239, in press
- Wedemeyer-Böhm, S., Steffen, M.: 2007, A&A 462, L31
- Wedemeyer, S., Freytag, B., Steffen, M., Ludwig, H.-G., Holweger, H.: 2004, A&A 414, 1121
- Wedemeyer-Böhm, S., Kamp, I., Bruls, J., Freytag, B.: 2005, A&A 438, 1043